Dyes and Pigments 94 (2012) 371–379

Contents lists available at SciVerse ScienceDirect

Dyes and Pigments

journal homepage: www.elsevier.com/locate/dyepig

Preparation of fluoroionophores based on diamine-salicylaldehyde derivatives

Wang-Hua Hong [a], Chu-Chieh Lin [a], Tung-Sheng Hsieh [b], Cheng-Chung Chang [b,*]

[a] Department of Chemistry, National Chung Hsing University, Taichung 250, Kuo Kuang Road, Taichung 402, Taiwan
[b] Graduate Institute of Biomedical Engineering, National Chung Hsing University 250, Kuo Kuang Road, Taichung 402, Taiwan

ARTICLE INFO

Article history:
Received 28 August 2011
Accepted 9 October 2011
Available online 20 October 2011

Keywords:
Fluoroionophore
DS (diamine-salicylaldehyde)
Metal recognizer
Anionic-dependent metal binding
Intermolecular complexation
Cellular metal staining

ABSTRACT

We have developed a series of fluoroionophores from diamine-salicylaldehyde (DS) derivatives and studied their spectra diversity when interacting with a variety of metal cations. Based on our results, 2-((*E*)-(2-(dimethylamino)ethylimino)methyl)-4-(4-methoxystyryl)phenol (**I**) can specifically chelate Zn^{+2} in both organic and semi-aqueous solution. Furthermore, 2-((*E*)-(2-(dimethylamino)ethylimino)methyl)-4-((*E*)-2-(pyridin-4-yl)vinyl)-phenol (**II**) is an excellent metal recognizer, successfully identifying Zn^{+2} from acetates, chloride and perchlorate salts. In addition, control compound (*E*)-N-(2-methoxy-5-((*E*)-2-(pyridin-4-yl)vinyl)benzylidene)-N′,N′-dimethyl-ethane-1,2-diamine (**IV**) also showed specific metal response to Cd^{+2} from $Cd(OAc)_2$ over other anions. This anionic-dependent metal binding behavior was imparted by the pyridine moiety, which supports extra intermolecular metal-fluorophore complexation. Fluoroionophores **I** and **II** were preliminarily tested for cellular metal staining in general fluorescence and ratio fluorescence methods.

1. Introduction

Among the chemosensors, fluorescent receptors have been actively investigated because of their high sensitivity [1]. In particular, fluorescent chemosensors that show a shift in emission upon binding with analytes are particularly attractive because they are not only capable of ratiometric sensing of analytes, but also offer advantages over conventional monitoring of fluorescence intensity at a single wavelength [2]. A dual emission system (one comes from the free fluorophore and another from complex) can minimize measurement errors from photo-transformation, receptor concentrations and environmental effects [3–5].

Metal ions are required for proper function of all cells within every living organism. For example, their careful regulation is important for aging and disease [6]. Thus, considering both the environmental and biological important, the development of materials and methods for the detection of heavy- and transition-metal cations is a synergistic advancement [7,8]. Sensors based on metal-induced changes in fluorescence appear to be particularly attractive as they offer the potential for high sensitivity at low analyte concentration coupled with their obvious ease of use [9,10]. Numerous fluorescent sensors for cations are known from the literature. These include chelators and even commercial materials [11–13]. Among them, the sensors with turn-on or ratiometric fluorescence signaling are particularly valuable [14–24]. However, to the best of our knowledge, there are no definite rules or platforms for screening these metal chelators based on their fluorophore. These considerations include: (i) why do the fluorescent enhancement phenomena happen in certain solvents or conditions? (ii) Once the metal chelator is sensitive to specific metal cations, what about its relative anionic effect? (i.e., most authors only care about whether the fluorophore chelator can bind to Zn^{+2}; few authors can illustrate the binding diversities between $ZnCl_2$, $Zn(OAc)_2$ or $Zn(ClO_4)_2$). (iii) Once the metal screening result from organic solutions is different from semi-aqueous or aqueous solution, which can be applied to predict cellular staining? Hence, establishing a research cascade including screening of fluorophores, determination of detection environments and the possibility of application to physiological diagnosis is critically important.

Schiff base is a well-known component of many chelators due to its electron-donating ability and adjustable coordination cavity [25,26]. The chelate center, which is constructed from symmetric or asymmetric ethylenediamine condensing with benzaldehyde derivatives, can form complexes with metals and show spectrum diversity. For example, a Cu^{+2} and Ni^{+2} sensor was constructed from 1-(2-aminoethylamino) anthracene-9, 10-dione and salicylaldehyde [27] as well as a 2-[(2-mercaptophenylimino) methyl] phenol (MPP) sensor that exhibited specific binding to Mg^{+2} [28]. The former showed different visible color changes upon addition of

* Corresponding author. Tel.: +886 4 22840734x24; fax: +886 4 228 52422.
E-mail address: ccchang555@dragon.nchu.edu.tw (C.-C. Chang).

0143-7208/$ – see front matter © 2011 Elsevier Ltd. All rights reserved.
doi:10.1016/j.dyepig.2011.10.007

metals, while the latter revealed a unique fluorescent response applied to quantum dot systems [29]. Furthermore, an ion exchange induced emission turn-on system was achieved when Hg^{+2} was added to Cu^{+2}-bis (2-hydroxyl-naphthalene-carboxaldehyde) benzyl dihydrazone (Cu^{+2}–H_2NB), a double Schiff base chelator [30].

In this paper, we report the preparation of diamine-salicylaldehyde (DS) as the chelator moiety from the condensation of N-N-dimethylethylenediamine and 2-hydroxybenzaldehyde (Salicylaldehyde) in advance. Two series of fluorophores were then constructed by conjugating DS chelators with aryl olefins (Scheme 1). Meanwhile, the hydroxyl of Salicylaldehyde was substituted with methyl to study its complexing and photophysical properties as a candidate for fluorescent chemosensors.

2. Experimental

2.1. Materials and apparatus

The general chemicals employed in this study were of the best grade available and were obtained from Acros Organic Co., Merck Ltd., or Aldrich Chemical Co. and used without further purification. All solvents were of spectrometric grade. Absorption spectra were generated using a *Thermo Genesys 6* UV–visible spectrophotometer, and fluorescence spectra were recorded using a *HORIBA JOBIN-YVON Fluoromas-4* spectrofluorometer with a 1-nm band-pass in a 1-cm cell length at room temperature.

2.2. Determination of quantum yields

The quantum yields of the DS derivatives were determined using the following equation [31]:

$$\Phi_{\mathbf{u}} = \Phi_{\mathbf{S}} \times \left[\mathbf{A_{fu}} \times \mathbf{A_s}(\lambda_{exs}) \times \eta_u^2\right] \Big/ \left[\mathbf{A_{fs}} \times \mathbf{A_u}(\lambda_{exu}) \times \eta_s^2\right]$$

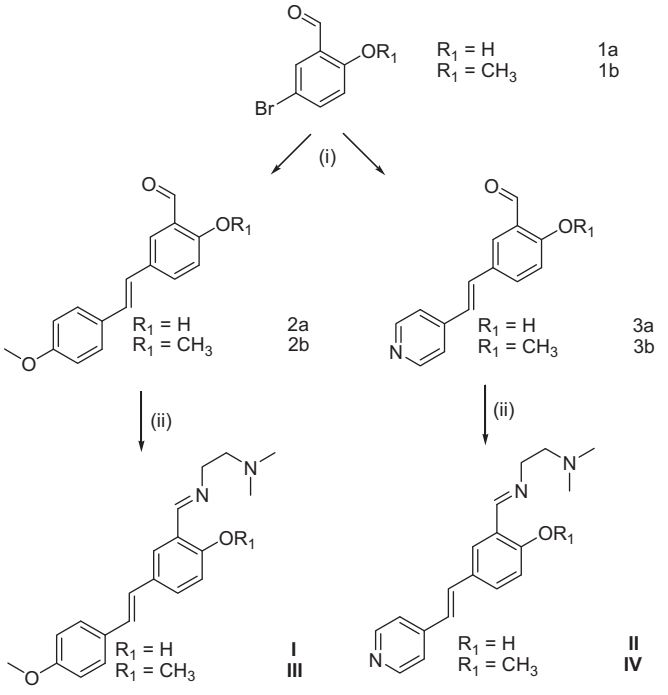

Scheme 1. Preparation of DS derivatives: (i) 4-vinyl aryl, $Pd(OAc)_2$, PPh_3, Et_3N, MeCN, reflux, 48 h; (ii) N,N-dimethylethylenediamine, MeOH, reflux, 12 h.

where $\Phi_{\mathbf{u}}$ is the quantum yield of unknown, $\mathbf{A_f}$ is the integrated area under the corrected emission spectra, $\mathbf{A}(\lambda_{ex})$ is the absorbance area at the excitation wavelength, η is the refractive index of the solution and the subscripts **u** and **s** refer to the unknown and the standard, respectively. For the same λ_{ex}, we chose Quinine sulfate as the standard, which has a quantum yield $\Phi = 0.58$ in DMSO (excitation 350 m).

2.3. Cell culture conditions and compound incubation

The MCF-7 human breast cancer cells were grown in Dulbecco's modified Eagle's medium (DMEM) with non-essential amino acid supplemented with 10% fetal calf serum (FCS). The human lung adenocarcinoma cell line CL1-0 was grown in RPMI 1640 (Gibco/Invitrogen™, Cat. no. 22400-089) medium containing 10% fetal bovine serum (FBS). Cell cultures were maintained at 37 °C in a humidified atmosphere of 95% air and 5% CO_2. The cells seeded in culture plates or dishes were incubated with different concentrations of DS derivatives, whose DMSO stock solutions were diluted in serum-free medium before use (1/100, v/v).

2.4. Cellular imaging

Before the observation of cellular localization, cells were seeded onto coverslips and incubated for 24 h. On the next day, cells were incubated with 10 μM of compound for 4 h, and then the fluorescence images were recorded on a *Leica AF6000* confocal fluorescence microscopy with a DFC310 FX Digital color camera. The λ scanning and fluorescence images were taken under a *Leica TCS SP5* confocal fluorescence microscopy. The excitation source was a 405 nm diode laser. Fluorescence photographs were taken through related ranges using photomultiplier tubes (PMT).

2.5. General procedure for the synthesis of diamine-salicylaldehyde derivatives (Scheme 1)

Synthesis of the DS derivatives is shown in Scheme 1. First, the phenol moiety of 5-bromosalicylaldehyde (compound **1a**) was methylated with iodomethane to afford compound **1b**. Next, the samples were subjected to Heck coupling reaction with 4-methoxystyrene or 4-vinylpyridine using $Pd(OAc)_2$ as the catalyst. Finally, Schiff base formation was conveniently performed with N,N-dimethylethylenediamine in methanol. Details of materials, synthetic procedures and identifications can be found in the Supporting Information.

3. Results and discussion

3.1. Molecular design and the focus of investigation

Herein, we constructed two fluorescent sensors by conjugating a DS chelator with 4-vinylanisole (compound **I**) and 4-vinylpyridine (compound **II**) (Scheme 1). The DS acted as the scaffold and the vinyl aryl acted to extend the electronic resonance. In general, incorporation of 4-vinylpyridine can support extra intermolecular binding ability to metal ions. That is, **II** may exhibit more binding modes than **I** when chelating with metal ions. Meanwhile, the hydroxyl group on DS was protected with methyl to generate the control compounds **III** and **IV** (from **I** and **II**, respectively). The purpose was to investigate if the metal-chelating properties were affected by the excited state intramolecular proton transfer (ESIPT) effect [29,32] as well as to estimate the contribution of the phenol group.

Another point of view on the compounds shown in Scheme 1 is that stilbene acts as the core scaffold and ethylene as the π-linker at

the center of the structure. The well-known intramolecular charge transfer (ICT) phenomenon, which is concerned with the donor-acceptor dipole moment exchange, should therefore be taken into account. This means that the dipole moment exchange, before and after chelating metal, would be the criteria to judge spectral diversity and in most of cases would be similar to protonation of the chelator. This is why most literatures reports (in Refs. [14–24]) mimic or predict the spectra diversity of a metal-fluorophore complex through protonation of the free fluorophore. In summary, we wish to ascertain whether ESIPT or ICT is the dominant factor in the design of a good metal chelator. Thus, the establishment of a metal screening platform in this manuscript included: (i) range determination of neutral structure (chelator) form [27,33]; (ii) solvent effect determination of free form and protonated form to check ICT variation; (iii) metal screening in optimal conditions based on results from (i) and (ii); and (iv) metal screening in under semi-aqueous or aqueous buffer systems to study the possibility of cellular application.

3.2. Basic spectroscopic properties and species distribution diagrams

The UV–visible absorption and fluorescence spectra of the obtained compounds were measured in DMSO and their optical data are presented in Table 1. Basically, the absorption energies of these compounds were located in the ultraviolet region with low quantum yields. On the other hand, the metal binding process is usually disturbed by protonation of fluorophore, so it is necessary to consider the pH effect and find optimal sensing conditions. In other words, protonation spectra of the chelator moiety in a variety of solvents might predict or mimic the spectra diversity of this compound with respect to solvent environment once bound to ions. Thus, we investigated the spectra responses of compounds toward pH in H_2O/MeOH (3:1) in advance to search for their fluorescent "turned on" states. Based on titration, spectrum deconvolution is important to find the distribution diagram of the neutral species actually playing the role of chelator. Fig. 1 shows the species distribution diagram for a system containing a solution of compounds **I** and **II** upon pH titration. L represents the neutral compound while deprotonation (protonation) of phenol (Schiff bases, vinylpyridine) is identified with pKa (pKb) value (Table 1).

3.3. Solvent effect and fluorescent enhancement of the protonated compound to mimic metal-chelating spectra

As mentioned above, protonation spectra of the chelator moiety in various solvents might predict or mimic the spectra diversity of a compound once binding to metal cations is complete. The UV–visible absorption and fluorescence spectra of the neutral and protonated forms of compounds **I** and **II** in variable organic solvents are presented in Fig. 2 (results of compounds **III** and **IV** are presented in Fig. S1). Regardless of the neutral or acidic condition, the absorption changes of both compounds **I** and **II** were insensitive to solvent polarity. These results clearly point toward a largely non-polar character for the ground state. However, the apparent red shift in the absorption maximum ($\lambda_{a\ max}$) of **II** under acidic conditions could be due to protonation of the pyridine moiety, increasing donor-accept effects. It is thus necessary and reasonable that the protonated behavior of pyridine should be taken into consideration since this functional group may be involved in the mechanism of metal chelation. On the other hand, considerable solvent effects in the fluorescence maximum ($\lambda_{f\ max}$) were observed in all cases. This hinted there was more polar character of excited states, which might have predominantly come from the ESIPT of DS derivatives. For applicable fluorescent sensors, colorful exchange and/or signal enhancement are required once they bind to their targets. Here, the solvent effect results in Fig. 2 were evaluated based on the criteria of apparent fluorescent enhancements. Compound **I** in DMF and MeOH and compound **II** in DMSO, MeOH and MeCN showed special emission enhancements, so these solvents were initially selected for the metal-chelating assay.

Further information regarding the dipole moment exchange between neutral and protonated compounds were previously collected [34]. In this study, the plots of ET(30) vs. Stokes shifts for these solvents are presented in Fig. 3 with a focus on the slope difference between neutral and protonated compounds. In an overall observation of the plots, unlike control compounds **III** and **IV**, whose ICT behaviors were definite and had no apparent difference between neutral and acidic environments, the plots of compounds **I** and **II** showed apparent and irregular differences between their neutral and protonated forms. Here, the deviations of the linear correlations were inferred due to (i) the phenol group of the DS moiety causing intramolecular hydrogen bonding (compounds **I** and **II**), demanding that the ESIPT effect should be counted; (ii) the pyridine group causing intermolecular hydrogen bonding (compound **II**). Hence, once the compound chelated with metals, it was temporally assumed that the spectral changes of **I** was the result of ESIPT effects, while **II** was the result of ICT and ESIPT effects.

3.4. Metal screening

To obtain a quantitative insight into the metal affinity of our fluorophore candidates, the wavelength changes upon complexation of various metal ions were determined. The solvent systems used were compound-dependent due to the criteria from solvent effects (Fig. 2) and the cation recognition behaviors of compounds were evaluated from changes in fluorescence intensities upon addition of metal-containing solutions (the final concentration of metal in the system was 400 μM). It must be pointed out that it is difficult to maintain the pH conditions of organic solvents, since most of these metal salts are acidic when dissolved in aqueous solution. Thus, the control assay was necessary to exclude the protonation effects from metal salts. For example, Fig. 4a shows the spectra changes of compound **I** upon addition of various metal ions in DMF. In a preliminary analysis of the fluorescence spectra results, most of metal ions were possibly responsive to **I**. Following the criterion of the protonated **I** (**I**–$\mathbf{H}^+$) curve in Fig. 4a, however, it was reasonable to assume that compound **I** chelated Zn^{2+} and Ag^+ in the DMF system. In contrast, control compound **III**, with the hydroxyl group absent, revealed no such significant change for any metal in the fluorescence spectrum under the same conditions. This revealed the importance of the hydroxyl group for chelation and showed that the phenol form was responsible for the binding of

Table 1
Photophysical properties of compounds **I** and **II**. Absorption (λ_{abs}, nm) and emission (λ_{em}, nm) maxima data were measured from DMSO solution; NMR data (chemical shift, ppm) were measured from DMSO-d6; pKa and pKb values were determined from H_2O/MeOH (3:1) solutions.

	λ_{abs} (ε)	λ_{em} (Φ_f)	^{1}H NMR		pKa, pKb		
			ArC<u>H</u>=N	Ar–O<u>H</u>	pKa1	pKb1	pKb2
I	318 (3.74)	420 (0.04)	8.549	13.703	10.20	5.10	–
II	325 (3.27)	433 (0.02)	8.556	13.398	9.59	5.33	4.70
III	318 (3.90)	425 (0.10)	8.632			5.42	
IV	321 (2.99)	390 (0.06)	8.639			5.51	4.52

λ_{abs}: absorption maximum (nm); ε: extinction coefficient ($\times$104, M^{-1} cm^{-1}); λ_{em}: emission maximum (nm); Φ_f: quantum yield (quinine sulfate, excitation 350 nm, $\Phi = 0.58$ as standard); pKa: deprotonation of phenol; pKb1: protonation of Schiff base; pKb2: protonation of vinylpyridine.

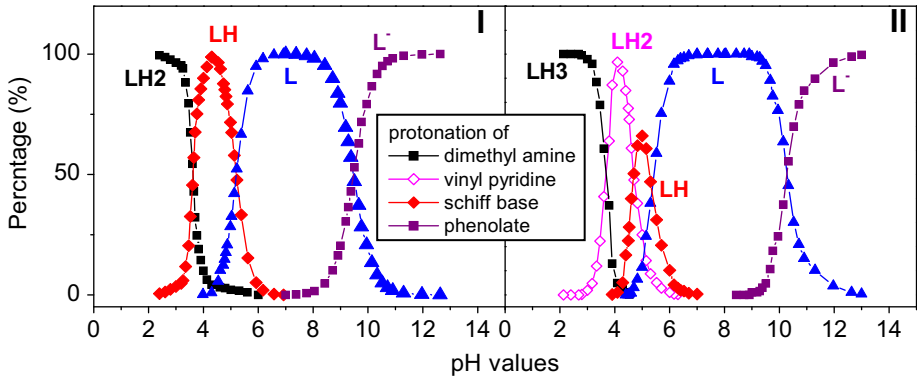

Fig. 1. pH-dependent relative species distribution diagrams of compounds **I** and **II**. Deprotonation of phenol and protonations of Schiff bases and vinylpyridine are identified with pKa and pKb values, respectively. L represents the neutral compounds.

metal through keto–enol tautomerism from the ESIPT mechanism. These data also established that the keto form was responsible for the effective binding of metals [28,35].

In an analogous inference in the case of solvent effects, compound **II** was tested for cation selectivity in DMSO and MeCN. The fluorescence spectrum of **II** showed marked enhancements at 480 nm with the addition of Zn^{2+} and less apparent fluorescent enhancement with Cd^{2+} (from $CdCl_2$ but not $Cd(OAc)_2$) and Hg^{2+} in DMSO with respect to the same concentration of HCl (Fig. 4b). The binding properties of **II** toward various metal ions in MeCN (Fig. 4c) were also evaluated and the results showed more complicated selectivity to Zn^{+2} (Fig. 4d). Initially, upon the addition of Zn^{2+} ions, only $Zn(OAc)_2$ could efficiently enhance the fluorescence intensity of **II** over other anions such as Cl^- and ClO_4^-; the emission band at 480 nm blue shifted to 470 nm and the intensity increased dramatically (~8.6 fold) when exciting the 315 nm λ_{max} absorption. While further investigation of the anion responses to the detection systems found that special emission bands at 550 nm grew when we excited either 380 or 430 nm, which belong to the unique absorption of **II**/$Zn(ClO_4)_2$ in MeCN (Fig. S2), there was no similar response to Cl^- or OAc^-. Combined with the Cd^{+2} case of Fig. 4b, it was clear that the anionic effect should also be included in the evaluation of the metal screening process. It seemed that compound **II** responded to the anionic effect, but not compound **I**.

Of note, binding properties of control compound **IV** showed a more selective response to Cd^{2+} of $Cd(OAc)_2$ than $CdCl_2$ in DMF (Fig. S3a) and to Zn^{2+} of $ZnCl_2$ (emission bands at 450 nm) and Cd^{2+} of $Cd(OAc)_2$ (emission bands at 442 nm) in MeCN (Fig. S3b). Even though we found that these fluorescence enhancements of **IV** were all lower then compound **II**, it was reasonable that these metal binding affinities or fluorescence enhancements of **IV** were less apparent than compound **II** due to the lack of ESIPT in compound **IV**, the same as in the case of control compound **III**. Nevertheless, based on these results, it was possible to infer that the pyridine group of compound **II** was the factor for anion-dependent metal binding behavior. The complete metal screening results are listed in the Table 2. From this table, fluoroionophore candidates with chelation enhanced fluorescence effects can be found. Consequently, we can screen solvent relative fluoroionophores that cannot only selectively chelate metal but also recognize this metal from other anions.

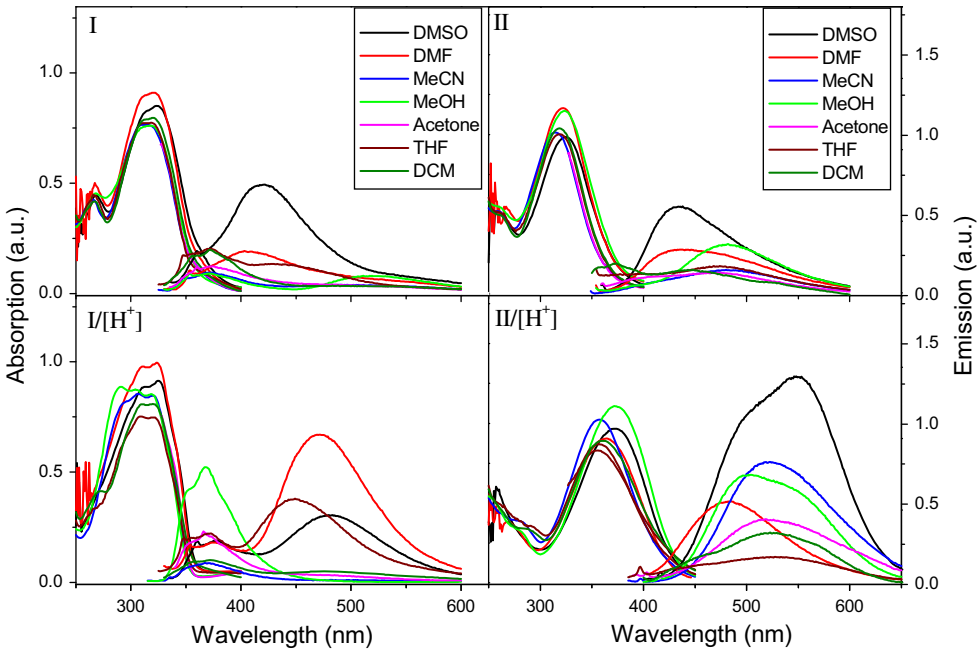

Fig. 2. UV–visible absorption and fluorescence spectra of 20 μM **I** and **II** in organic solvents under neutral and acidic conditions (12 mM $[H^+]$); absorption λ_{max} is the excited wavelength.

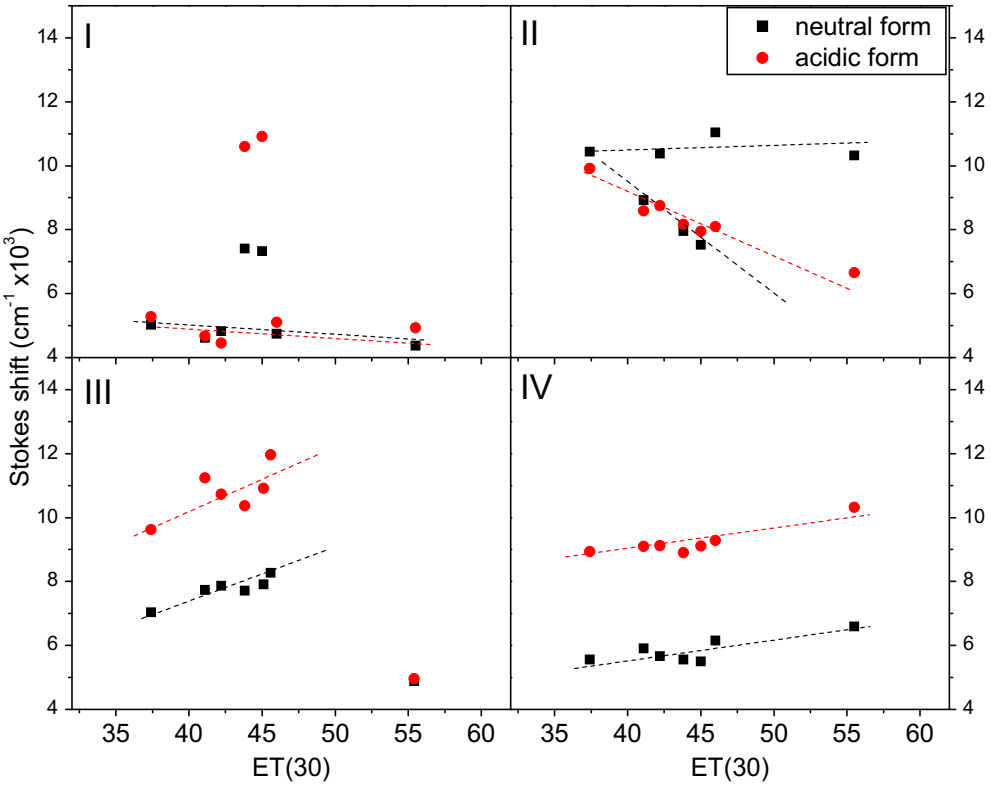

Fig. 3. The plots of solvent polarity (ET(30)) vs. Stokes shifts using the results in Fig. 2 and Fig. S1.

3.5. Metal screen in a semi-aqueous system

After systematically looking for selective behavior toward different metal ions for potential biosensor applications, fluorescence measurements were collected in a semi-aqueous system at 25 °C (H_2O/MeOH = 3:1, pH ~ 7.0 HEPES buffer, [**I**] = 20 μM and [M] = 400 μM). As shown in Fig. 5a, free compound **I** typically showed emission bands at 370 nm and 550 nm with very

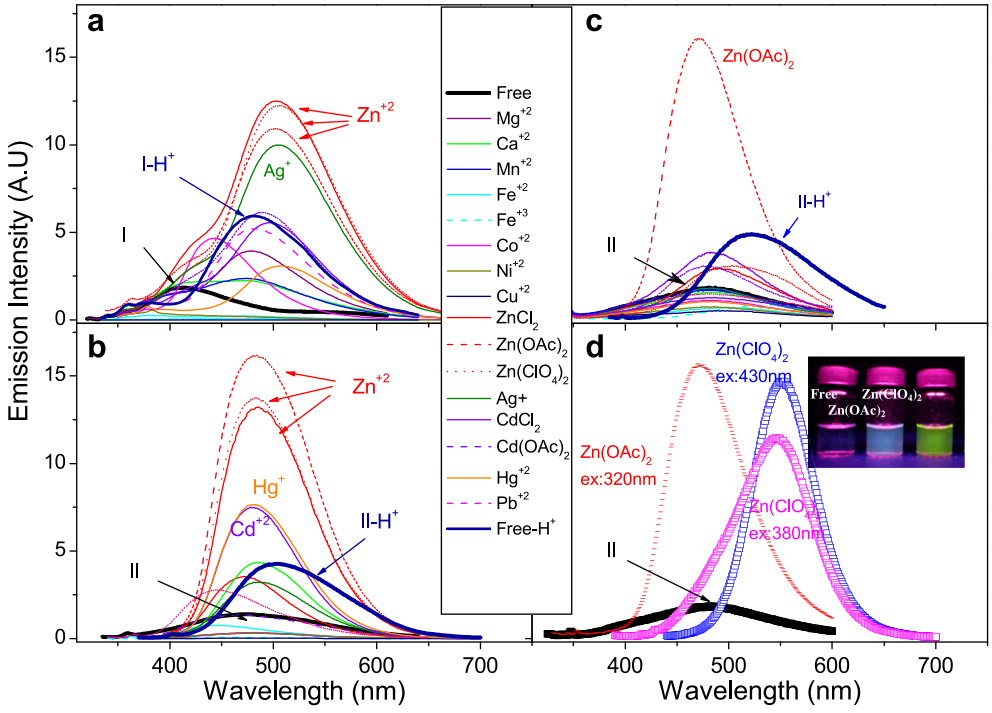

Fig. 4. Metal screening fluorescence spectra of 20 μM (a) **I** in DMF, (b) **II** in DMSO, (c) **II** in MeCN and (d) **II** in MeCN by exciting the relative absorption of compound in $Zn(ClO_4)_2$. Metal salts: $MgCl_2$, $CaCl_2$, $MnSO_4$, $FeCl_2$, $FeCl_3$, $Co(OAc)_2$, $Ni(OAc)_2$, $Cu(OAc)_2$, $ZnCl_2$, $Zn(OAc)_2$, $Zn(ClO_4)_2$, $AgNO_3$, $CdCl_2$, $Cd(OAc)_2$, $HgCl_2$ and $Pb(NO_3)_2$ were used in this study. The excited wavelength is absorption maxima.

Table 2
Optical response of fluoroionophore candidates **I**, **II** and **IV** (20 μM) to different metal salts (400 μM). Numbers in the table represent the relative fluorescent enhancement with respect to the metal-free system.

	Zn^{+2} (Cl^-)	Zn^{+2} (OAc^-)	Zn^{+2} (ClO_4^-)	Ag^+	Cd^{+2} (Cl^-)	Cd^{+2} (OAc^-)	Hg^{+2}
I (DMF)	6.6	6.5	5.8	5.3			
I (H_2O/MeOH)	11.7	9.6	8.7				
II (DMSO)	9.5	9.8	11.5		5.36		5.48
II (H_2O/MeOH)	3.5	3.9	3.2		4.19	3.54	
II (MeCN)		8.6	7.7[a]				
			6.0[b]				
IV (DMF)						3.00	
IV (MeCN)	4.3					3.30	

[a] Excited wavelength = 430 nm.
[b] Excited wavelength = 380 nm.

low intensities under these conditions. Fluorescent enhancement at 514 nm was observed with addition of Zn^{2+}, however, no increase in fluorescent emission was seen with other metal ions. Moreover, the binding selectivity was anion independent since the detection systems all in response to $ZnCl_2$, $Zn(OAc)_2$ and $Zn(ClO_4)_2$. Meanwhile, absorption spectra of these metal-containing solutions showed no apparent differences and stayed in the UV region with no distinct color change in the solution. Compound **II** showed anion independent selectivity to Zn^{2+} and Cd^{2+} under the same conditions with fluorescent enhancement from 510 nm to 500 nm and 520 nm, respectively. In particular, there were apparent red shifts in the absorption bands (Fig. 5b) and this case was similar to the results from solvent effects for protonated **II** (Fig. 2).

In this semi-aqueous buffer solution, protonation of pyridine should be excluded. Hence, the phenomenon of absorption red shifts was likely the result of the pyridine of compound **II** becoming involved in the metal-chelating mode. That is, an extra intermolecular binding mode was possible for compound **II** to chelate metal ions and support extra coordinate binding to anion to form metal cation-anion-fluorophore complexes. Moreover, metal-chelating behaviors were proposed to arise from the competition between solvation of salts and complexation of metals to the fluorophore. This hypothesis explained that anion-dependent metal-chelating behaviors should only be observed in organic solvent.

3.6. Illustration of binding mode

To gain more insight into the chemosensing properties and mechanisms of these metal-chelating fluorophores toward metal ions, absorption and fluorescence titrations of compounds with metal ions in semi-aqueous buffer solution (H_2O/MeOH = 3:1 (v/v), pH ~ 7.0 HEPES buffer) were carried out. In the fluorescence emission of **I** at 20 μM when adding $Zn(ClO_4)_2$ from 2 to 80 μM, we observe that a weak fluorescence peak shifted from 360 and 560 to 510 nm, gradually increasing in intensity. Under similar conditions, upon the gradual addition of $Cd(OAc)_2$ from 0 to 4 equivalents, the λ_{em} of **II** underwent a red shift from 510 nm to 520 nm and a 4-fold fluorescence enhancement was also observed. The titration conditions and results are shown in Fig. S4. Regardless of absorption or emission titration spectra, there was more than one isosbestic point indicating that the binding behaviors were not a single step.

The strong enhancement of the fluorescence upon interaction with metals allowed us to study the binding using fluorescence titration at low concentration. In this type of study, the Scatchard binding model determines the number(s) of equivalent binding sites and the affinities of ligands for those sites ($\gamma/Cf = nK - \gamma K$) [36,37]. These titration data were then applied to construct the binding plots of γ vs. *Cf*. The binding ratio γ is defined as *Cb*/Cm, where *Cf*, *Cb*, and *Cm* are the molar concentrations of free ligand, bound ligand, and metal, respectively. In our Scatchard analysis, the difference between *Ct* (total concentration of ligand) and *Cb* gave the magnitude of *Cf*. The slightly non-linear Scatchard plots in Fig. 6a used for obtaining both *K* and *n* values became irrelevant [38] and indicated again that the binding was not a single step. Here, the *K* values for **I** to Zn^{+2} were 2.91×10^6 and 3.41×10^5 mol^{-1} with $n \sim 1.04$ and ~1.88. It was thus reasonable that a larger value of γ at low concentrations of Zn^{+2} was probably due to a 2:1 **I**: Zn^{+2}

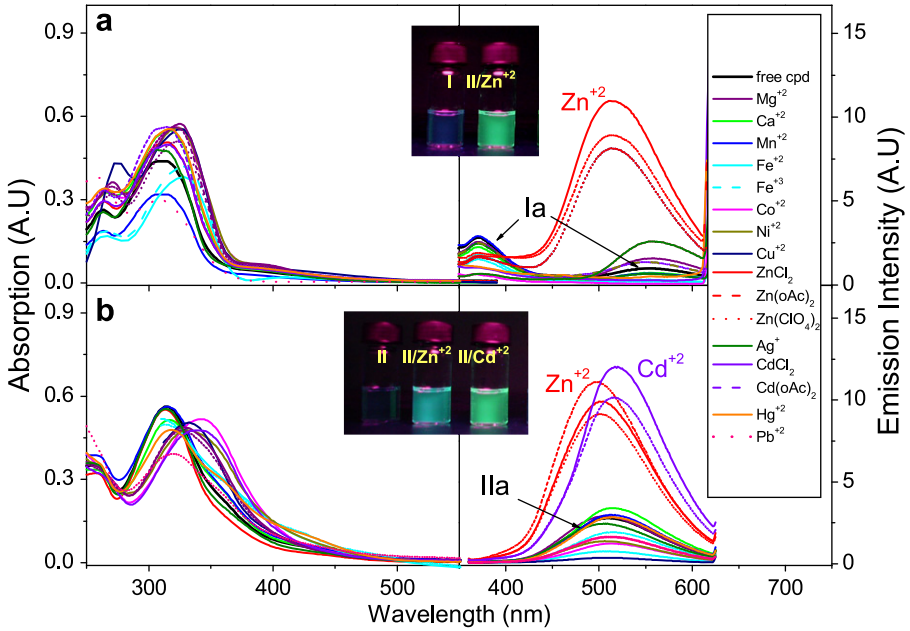

Fig. 5. Metal screening absorption (left) and fluorescence (right) spectra of 20 μM (a) **I** and (b) **II** in a semi-aqueous system at 25 °C (H_2O/MeOH = 3:1, pH ~7.0 HEPES buffer, [M] = 400 μM). The excited wavelength is absorption maxima.

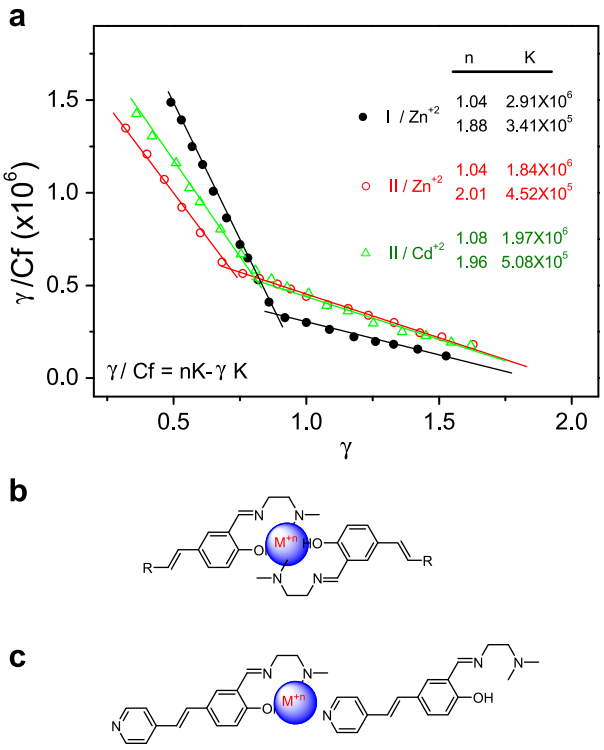

Fig. 6. (a) Binding constant and binding ratio illustrations for **I** to zinc and **II** to zinc and cadmium. The Scatchard plots were based on the titration results shown in Fig. S4 with elimination of unreasonable data. (b) Possible head-to-head binding mode for compound:metal (blue ball) = 2:1. (c) Possible head-to-tail binding mode for compound:metal = 2:1. (For interpretation of the references to color in this figure legend, the reader is referred to the web version of this article.)

binding ratio and binding modes as proposed in Fig. 6b (i.e., head-to-head mode).

In another case, the K values for **II** to Zn^{+2} were 1.84×10^6 and 4.52×105 mol^{-1} with $n \sim 1.04$ and ~ 2.11; the K values for **II** to Cd^{+2} were 1.97×10^6 and 5.08×10^5 mol^{-1} with $n \sim 1.08$ and ~ 1.96. These results for **II** revealed that the more than one binding ratio was dominant due to its larger region of titration and non-linear Scatchard curves. Together with its apparent red shift of absorption within the titration process, we inferred that the pyridine moiety of **II** took part in the chelating process. Consequently, the binding modes of **II** to metal ions involve the binding modes seen in Fig. 6b and c (i.e., head-to-tail mode).

3.7. Application as biosensor of cellular imaging

Following the results from semi-aqueous systems, the cell permeability of compounds **I** and **II** was determined. Breast cancer cell line MCF-7 was incubated with compounds (10 μM) and the increase of fluorescence intensity in living cells was observed upon addition of metal salts (Zn^{+2} or Cd^{+2}, 50 μM) into the medium with incubation for 1 h at 37 °C. Similar cellular fluorescent enhancement was also observed when cells were exposed to 50 μM of metal salts for 4 h and then further incubated with 10 μM compounds for 2 h at 37 °C. The images were obtained on a fluorescence microscopy with a digital color camera and excited by a blue light cube (Fig. 7). Regardless of metal pre-incubation or post-incubation, the penetration and intracellular metal sensing of **I** and **II** were very clear.

The fluorescence images of intracellular metal ions were further observed under a confocal microscope. In order to apply 405 nm diode laser irradiation, the cell staining concentrations of compounds I and II were increased to 20 μM because their absorption wavelengths were lower then 400 nm. Fig. 8a shows negligible fluorescence when lung adenocarcinoma cells CL1-0 were incubated with I for 2 h at 37 °C, but fluorescence enhancement was observed from the addition of $ZnCl_2$ (50 μM) into the medium with incubation for another 1 h at 37 °C (Fig. 8b). In addition, evaluation of the λ scanning spectra suggested that the λ_{max} of the emission wavelength (~510 nm, Fig. 8c) was very close to the spectrum of a Zn^{+2}-fluorophore complex in semi-aqueous solution (Fig. 5a). Similar results were also observed when II-incubated cells were treated with $ZnCl_2$ (Fig. 8e) and $CdCl_2$ (Fig. 8f), but the λ_{max} (~530 nm) of the emission wavelength from the λ scanning spectra was longer than that in semi-aqueous condition (Fig. 5b). These differences were proposed to be the result of cellular environment of II stay being more hydrophobic or that aggregation occurred. Nevertheless, the results suggested that **I** and **II** could be used to image intracellular Zn^{+2} or Cd^{2+} in living cells using both general fluorescence and ratio fluorescence methods. These compounds are thus potentially useful for the study of the toxicity or bioactivity of metal ions in living cells.

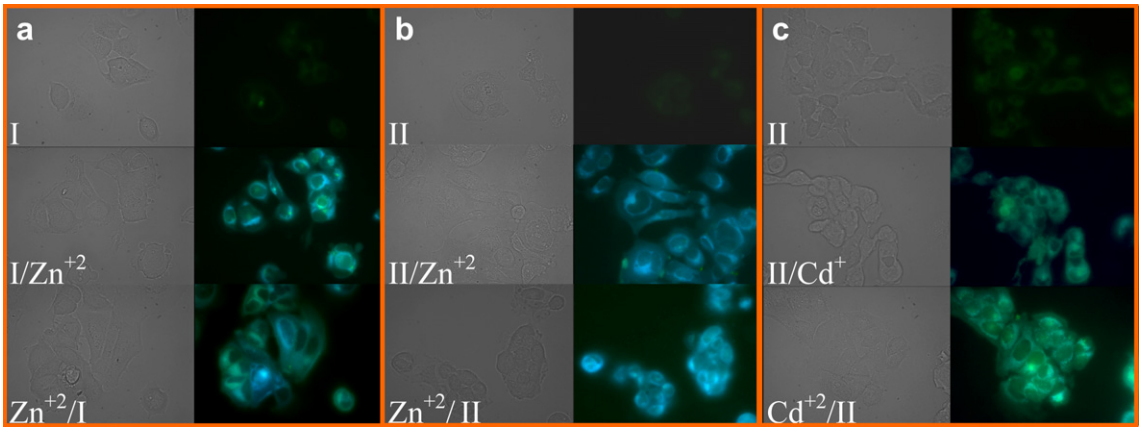

Fig. 7. The bright field images (left) and fluorescence images (right) from fluorescence microscopy for (a) **I**–Zn^{+2}, (b) **II**–Zn^{+2} and (c) **II**–Cd^{+2} systems. MCF-7 cancer cells were incubated with 10 μM compounds (upper) and then 50 μM metal salts were added into the medium and incubation for 1 h at 37 °C (middle). Cells were exposed to 50 μM metal salts for 4 h and then further incubated with 10 μM compounds for 2 h at 37 °C (bottom). The images were excited by a blue light cube light path through a 370/20 nm band-pass filter and emission was collected and filtered through a 450-nm long-pass filter. (For interpretation of the references to color in this figure legend, the reader is referred to the web version of this article.)

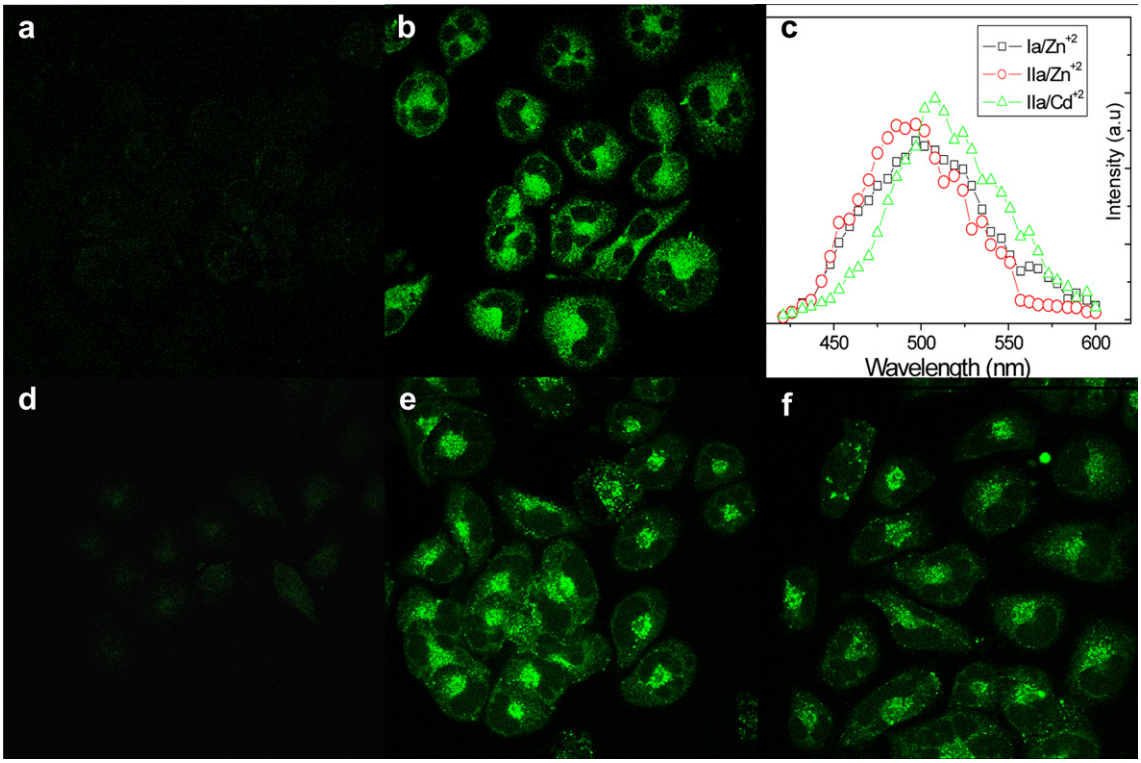

Fig. 8. Confocal fluorescence images of **I** and **II** in CL1-0 cells. The excitation light is 405 nm, and the collected wavelength ranged from 450 to 650 nm. Fluorescence images of CL1-0 cells were incubated with **I** (a) or **II** (d) for 2 h, washed, and then further incubated with 50 μM $ZnCl_2$ (b), (e) or $CdCl_2$ (f) for 1 h. (c) Normalized λ scanning spectra from 420 to 600 nm with 10 nm integration of (b), (e) and (f).

4. Conclusions

To develop a set of available fluorescence sensors, optimized chelating conditions for the DS derivatives studied here were evaluated by observing their ESIPT and ICT behaviors through pKa measurement and solvent effect assays. Together with data from the control compounds, ESIPT was found to be necessary for a compound to become a metal chelator and ICT was necessary for a metal chelator to have a color shift and/or signal enhancement. Consequently, fluoroionophore **I** displayed specific binding to Zn^{+2}, and fluoroionophore **II** could not only chelate Zn^{+2} or Cd^{+2} but also had anion-dependent metal binding behavior in organic solvents. Finally, **I** and **II** were applied to the identification of Zn^{+2} and Cd^{+2} in cells after evaluating their metal binding selectivity in semi-aqueous systems.

Acknowledgments

This work was supported financially by the National Science Council (NSC 99-2113-M-005-011-MY2) of Taiwan.

Appendix. Supplementary material

Supplementary material associated with this article can be found, in the online version, at doi:10.1016/j.dyepig.2011.10.007.

References

[1] de Silva AP, Gunaratne HQN, Gunnlaugsson T, Huxley AJM, McCoy CP, Rademacher JT, et al. Signaling recognition events with fluorescent sensors and switches. Chem Rev 1997;97:1515–66.
[2] Lakowicz JR. Topics in fluorescence spectroscopy. In: Probe design and chemical sensing, vol. 4. New York: Plenum Press; 1994.
[3] Grynkiewicz G, Poenie M, Tsien RY. A new generation of Ca^{2+} indicators with greatly improved fluorescence properties. J Biol Chem 1985;260:3440–50.
[4] Banthia S, Samanta A. A new strategy for ratiometric fluorescence detection of transition metal ions. J Phys Chem B 2006;110:6437–40.
[5] Jung HJ, Singh N, Jang DO. Highly Fe^{3+} selective ratiometric fluorescent probe based on imine-linked benzimidazole. Tetrahedron Lett 2008;49:2960–4.
[6] Lippard SJ, Berg JM. Principles of bioinorganic chemistry. Mill Valley, California, USA: University Science Books; 1994. 139–175.
[7] Denk W, Strickler JH, Webb WW. 2-photon laser scanning fluorescence microscopy. Science 1990;248:73–6.
[8] Lichtman JW, Conchello JA. Fluorescence microscopy. Nat Methods 2005;2: 910–9.
[9] Lakowicz JR. Principles of fluorescence spectroscopy. 3rd ed. New York: Springer; 2006.
[10] Domaille DW, Que EL, Chang CJ. Synthetic fluorescent sensors for studying the cell biology of metals. Nat Chem Biol 2008;4:168–75.
[11] Palacios MA, Wang Z, Montes VA, Zyryanov GV, Hausch BJ, Jursıkova K, et al. Hydroxyquinolines with extended fluorophores: arrays for turn-on and ratiometric sensing of cations. Chem Commun; 2007:3708–10.
[12] Callan JF, de Silva AP, Magri DC. Luminescent sensors and switches in the 21st century. Tetrahedron 2005;61:8551–88.
[13] Valeur B, Leray I. Design principles of fluorescent molecular sensors for cation recognition. Coord Chem Rev 2000;205:3–40;
Lee JW, Lee JS, Kang M, Su AI, Chang YT. Visual artificial tongue for quantitative metal cation analysis by an off-the-shelf dye array. Chem Eur J 2006;12: 5691–6.
[14] Woodroofe CC, Lippard SJ. A novel two-fluorophore approach to ratiometric sensing of Zn^{2+}. J Am Chem Soc 2003;125:11458–9.
[15] Royzen M, Durandin A, Young Jr VG, Geacintov NE, Canary JW. A sensitive probe for the detection of Zn(II) by time-resolved fluorescence. J Am Chem Soc 2006;128:3854–5.
[16] Maruyama S, Kikuchi K, Hirano T, Urano Y, Nagano T. A novel, cell-permeable, fluorescent probe for ratiometric imaging of zinc ion. J Am Chem Soc 2002; 124:10650–1.
[17] Qi X, Jun EJ, Xu L, Kim SJ, Hong JSJ, Yoon YJ, et al. New BODIPY derivatives as off-on fluorescent chemosensor and fluorescent chemodosimeter for Cu^{2+}: cooperative selectivity enhancement toward Cu^{2+}. J Org Chem 2006;71: 2881–4.
[18] Nolan EM, Lippard SJ. A "turn-on" fluorescent sensor for the selective detection of mercuric ion in aqueous media. J Am Chem Soc 2003;125: 14270–1.
[19] Yoon S, Albers AE, Wong AP, Chang CJ. Screening mercury levels in fish with a selective fluorescent chemosensor. J Am Chem Soc 2005;127:16030–1.

[20] Hirano T, Kikuchi K, Urano Y, Nagano T. Improved fluorescent probes for zinc, ZnAFs, suitable for biological applications. J Am Chem Soc 2002;124: 6555–62.
[21] Wu Y, Peng X, Guo B, Fan J, Zhang Z, Wang J, et al. Boron dipyrromethene fluorophore based fluorescence sensor for the selective imaging of Zn(II) in living cells. Org Biomol Chem 2005;3:1387–92.
[22] Peng X, Du J, Fan J, Wang J, Wu Y, Zhao J, et al. A selective fluorescent sensor for imaging Cd^{2+} in living cells. J Am Chem Soc 2007;129:1500–1.
[23] Ha-Thi MH, Penhoat M, Michelet V, Leray I. Highly selective and sensitive phosphane sulfide derivative for the detection of Hg^{2+} in an organoaqueous medium. Org Lett 2007;9:1133–6.
[24] Taki M, Desaki M, Ojida A, Iyoshi S, Hirayama T, Hamachi I, et al. Fluorescence imaging of intracellular cadmium using a dual-excitation ratiometric chemosensor. J Am Chem Soc 2008;130:12564–5.
[25] Lewinski J, Zachara J, Justyniak I, Dranka M. Hydrogen-bond supramolecular structure of group 13 Schiff base complexes. Coord Chem Rev 2005;249: 1185–99.
[26] Chen HY, Tang HY, Lin CC. Ring-opening polymerization of lactides initiated by zinc alkoxides derived from NNO-tridentate ligands. Macromolecules 2006;39:3745–52.
[27] Kaur N, Kumar S. Single molecular colorimetric probe for simultaneous estimation of Cu^{2+} and Ni^{2+}. Chem Commun 2007;29:3069–70.
[28] Singh N, Kaur N, Mulrooney RC, Callan JF. A ratiometric fluorescent probe for magnesium employing excited state intramolecular proton transfer. Tetrahedron Lett 2008;49:6690–2.
[29] Singh N, Mulrooney RC, Kaur N, Callan JF. A nanoparticle based chromogenic chemosensor for the simultaneous detection of multiple analytes. Chem Commun; 2008:4900–2.
[30] He G, Zhao Y, He C, Liu Y, Duan C. "Turn-on" fluorescent sensor for Hg^{2+} via displacement approach. Inorg Chem 2008;47:5169–76.
[31] Vieira Ferreira LF, Costa SMB. Fluorescence quantum yield evaluation of strongly absorbing dye solutions as a function of the dye concentration. J Lumin 1991;48–49:395–9.
[32] Hadjoudis E, Mavridis IM. Photochromism and thermochromism of Schiff bases in the solid state: structural aspects. Chem Soc Rev 2004;33:579–88.
[33] Tang XL, Peng XH, Dou W, Mao J, Zheng JR, Qin WW, et al. Design of a semi-rigid molecule as a selective fluorescent chemosensor for recognition of Cd(II). Org Lett 2008;10:3653–6.
[34] Loutfy RO, Arnold BA. Effect of viscosity and temperature on torsional relaxation of molecular rotors. J Phys Chem 1982;86:4205–11.
[35] Bhardwaj VK, Singh N, Hundal MS, Hundal G. Mesitylene based azo-coupled chromogenic tripodal receptors-a visual detection of Ag(I) in aqueous medium. Tetrahedron 2006;62:7878–86.
[36] Hollemans HJG, Bertlna RM. Scatchard plot and heterogeneity in binding affinity of labeled and unlabeled ligand. Clin Chem 1975;21:1769–73.
[37] Chang CC, Wu JY, Chien CW, Wu WS, Liu H, Kang CC, et al. A fluorescent carbazole derivative: high sensitivity for quadruplex DNA. Anal Chem 2003; 75:6177–83.
[38] Chaires JB. Analysis and interpretation of ligand-DNA binding isotherms. Meth Enzymol 2001;340:3–22.